JNeurosci
THE JOURNAL OF NEUROSCIENCE

Research Report: Regular Manuscript

Cross-frequency phase-amplitude coupling between hippocampal theta and gamma oscillations during recall destabilizes memory and renders it susceptible to reconsolidation disruption

https://doi.org/10.1523/JNEUROSCI.0259-20.2020

Cite as: J. Neurosci 2020; 10.1523/JNEUROSCI.0259-20.2020

Received: 3 February 2020
Revised: 24 June 2020
Accepted: 29 June 2020

Behavioral/Cognitive

Cross-frequency phase-amplitude coupling between hippocampal theta and gamma oscillations during recall destabilizes memory and renders it susceptible to reconsolidation disruption

Abbreviated title: **Hippocampal rhythms and memory reconsolidation**

Andressa Radiske[1,†], Maria Carolina Gonzalez[1,†], Sergio Conde-Ocazionez[2], Janine I. Rossato[1,3], Cristiano A. Köhler[1], and Martín Cammarota[1,*]

[1]Memory Research Laboratory, Brain Institute, Federal University of Rio Grande do Norte, Av. Nascimento de Castro 2155, RN 59056-450, Natal, Brazil. [2]School of Medicine, University of Santander, Campus Universitário Lagos del Cacique, Calle 70, 55-210, Bucaramanga, Colombia. [3]Departament of Physiology, Federal University of Rio Grande do Norte, Av. Sen. Salgado Filho 3000, RN 59064-741, Natal, Brazil. [†]Equally contributed. *Address correspondence to Martín Cammarota at martin.cammarota@neuro.ufrn.br.

Number of pages: 32
Number of figures: 5
Number of tables: 1
Number of words for Abstract: 136
Number of words for Introduction: 453
Number of words for Discussion: 653

Conflict of Interest. The authors declare no competing financial interests.

Acknowledgments

This study was supported by Conselho Nacional de Desenvolvimento Científico e Tecnológico (CNPq, Brazil) and Coordenação de Aperfeiçoamento de Pessoal de Nível Superior (CAPES, Brazil). We thank Jorge H. Medina for helpful discussion.

Abstract

Avoidance memory reactivation at recall triggers hippocampal theta-gamma phase amplitude coupling (hPAC) only when it elicits hippocampus-dependent reconsolidation. However, it is not known whether there is a causal relationship between these phenomena. We found that in adult male Wistar rats, silencing the medial septum during recall did not affect avoidance memory expression or maintenance but abolished hPAC and the amnesia caused by the intra-hippocampal administration of reconsolidation blockers, both of which were restored by concomitant theta burst stimulation of the fimbria-fornix pathway. Remarkably, artificial hPAC generated by fimbria-fornix stimulation during recall of a learned avoidance response naturally resistant to hippocampus-dependent reconsolidation made it susceptible to reactivation-dependent amnesia. Our results indicate that hPAC mediates the destabilization required for avoidance memory reconsolidation, and suggest that generation of artificial hPAC at recall overcomes the boundary conditions of this process.

Significance Statement

Hippocampal theta-gamma phase-amplitude coupling (hPAC) increases during the induction of hippocampus-dependent avoidance memory reconsolidation. However, whether hPAC plays a causal role in this process remains unknown. Using behavioral, electrophysiological, optogenetic and biochemical tools in adult male Wistar rats, we demonstrate that reactivation-induced hPAC is necessary for avoidance memory destabilization, and that artificial induction of this patterned activity during recall of reconsolidation-resistant aversive memories renders them liable to the amnesic effect of reconsolidation inhibitors.

Introduction

Memories are initially susceptible to disruption but, as time passes, they consolidate and become resistant to interference (McGaugh, 1966; Dudai, 2004). Nevertheless, reactivation during recall can destabilize consolidated memories, which must then be restabilized through a gene expression and protein synthesis-dependent reconsolidation process in

order to persist (Spear, 1973; Przybyslawski and Sara, 1997; Nader et al., 2000, Haubrich and Nader, 2018).

Post-traumatic stress disorder (PTSD) is a highly prevalent mental illness triggered by witnessing or suffering distressing events (Bryant, 2019). PTSD patients show exacerbated avoidance when face situations reminding the trauma, and are usually treated with anxiolytic or antidepressant medication in combination with psychotherapy (Pratchett et al., 2011; Polak et al., 2012; Friedman and Bernardy, 2017), although the relapse and recurrence rates are high (Batelaan et al., 2017). Because reconsolidation may mediate the incorporation of new information into unstable reactivated memories (Nader and Hardt, 2009; Nader and Einarsson, 2010; Haubrich and Nader, 2018), clinical interventions able to destabilize avoidance memories and enable their reconsolidation could help PTSD patients to resignify aversive recollections and recontextualize traumatic experiences (Schwabe et al., 2014; Elsey and Kindt, 2017; Dunbar and Taylor, 2017; Waits and Hoge, 2018). However, reactivation at recall does not necessarily destabilize memory (Cammarota et al., 2004; Sevenster et al., 2012; Merlo et al., 2014; Bos et al., 2014; Thome et al., 2016), but there are conditions that constrain this process and limit the occurrence of reconsolidation (Nader and Hardt, 2009).

Oscillatory activity is a fundamental property of brain function (Buzsáki, 2006). In particular, the hippocampus shows prominent oscillations in the theta and gamma frequency bands (Buzsáki, 2002; Colgin et al., 2009). Theta and gamma oscillations interact with each other (Lisman and Jensen, 2013). In fact, gamma amplitude is modulated by the phase of theta (Jensen and Colgin, 2007), and it is theorized that theta-gamma phase-amplitude coupling (hPAC) coordinates neuronal activity at the timescale required for memory processing in the hippocampus (Skaggs et al., 1996; Lisman et al., 2005), although the actual role of this interaction remains unclear (Lisman and Buzsáki, 2008). In this respect, hPAC strength predicts correct choice probability over the course of associative learning (Tort et al., 2009) and increases when animals evaluate choice-relevant information (Amemiya and Redish, 2018), which seems to be essential for the destabilization of some memory types at the

moment of recall, including avoidance memory (Radiske et al., 2017; Yang et al., 2019). Interestingly, we recently showed that hPAC strength is associated with hippocampus-dependent avoidance memory reconsolidation in rats (Radiske et al., 2017). Here, we determined that there is a causal relationship between hPAC induction and avoidance memory destabilization, and demonstrated that generation of artificial hPAC during retrieval can make reconsolidation-resistant avoidance memories susceptible to reactivation-targeted amnesic manipulations.

Materials and Methods

Subjects

We used a total of 785 3-month-old naïve male Wistar rats weighing 300-350 g, including those utilized for pilot experiments. They were maintained in a vivarium on a 12:12 h light/dark cycle (lights on at 06:00 AM) at 23°C and housed in groups of 5 per cage with free access to food and water. Experiments were performed during the light phase of the cycle and conducted by researchers blinded to the animals' behavioral condition and treatment. Procedures were in accordance with the USA National Institutes of Health Guidelines for Animal Care and were approved by the local institutional ethics committee (Comissão de Ética no Uso de Animais - CEUA).

Surgical procedures

Anesthetized rats (ketamine 80 mg/kg; xylazine 10 mg/kg) were implanted with 22-gauge stainless steel guide cannulas aimed at the CA1 region of the dorsal hippocampus (AP, −4.2; LL, ±3.0; DV, −3.0 in mm) and/or the medial septum (MS; AP, -0.2; LL, -1.1; DV, -6.0 in mm; 10° angle insertion). For experiments involving electrical stimulation of the fimbria-fornix (FFx) or the corpus callosum, bipolar electrodes were lowered to AP, -1.3; LL, +1.4; DV, -4.0 or AP, -1.3; LL, +1.4; DV, -3.0 coordinates, respectively. For optogenetically silencing the MS, we delivered the adeno-associated viral vector AAV-CAG-ArchT-GFP (UNC Vector Core; 2×10^{11} particles/ml) using a Hamilton syringe coupled to an infusion pump (3 x 0.5 µl

at a rate of 0.2 µl/min) aimed at three consecutive depths in the MS (AP, -0.2; LL, -1.1; DV,-5.5/-6.0/-6.5 in mm; 10° angle insertion). Two weeks later, optical fibers (200-µm diameter) were implanted in the MS. To record hippocampal LFPs signals, animals were implanted with sixteen-channel electrode arrays (50 µm tungsten wires coated with PFA arranged in a 2x8 250 µm-spaced configuration) aimed to dorsal CA1 (AP, −3.6; LL, +2.4; DV, −3.6 mm). Two screws were twisted into the parietal bone to establish ground connection. Stereotaxic coordinates were chosen based on previous reports (Shirvalkar et al., 2010; Radiske et al., 2017). After surgery, animals received subcutaneous meloxicam (0.2 mg/kg). Rats implanted with electrode arrays were housed individually. Experiments began no less than 10 days after surgery.

Drugs and infusion procedures

Drug doses were based on previous studies and pilot experiments. C/EBPβ antisense (5'-CCAGCAGGCGGTGCATGAAC-3′; 2 nmol/µl) and C/EBPβ scrambled antisense oligonucleotides (5'-TCGGAGACTAAGCGCGGCAC-3′; 2 nmol/µl) were phosphorothioated on the three terminal bases to avoid nuclease degradation. Oligonucleotides, anisomycin (160 µg/µl), and muscimol (0.2 µg/µl) were dissolved upon arrival, aliquoted and stored at −20 °C until use. Stock aliquots were thawed and diluted to working concentration in sterile saline (pH ~7.2) on the day of the experiment. For intra-cerebral drug delivery, infusion cannulas were fitted into the guides, and infusions carried out using a Hamilton syringe coupled to an infusion pump (1 µl/side at a rate of 0.5 µl/min and 0.5 µl at a rate of 0.25 µl/min for intra-dorsal CA1 and intra-MS infusions, respectively). Infusion cannulas were left in place for one additional minute to minimize backflow.

Habituation

Before the experiments involving optogenetic/electrical stimulation and/or electrophysiological recordings, animals were habituated to mounting the optic fiber, the stimulator connector and/or the headstage without anesthesia, and to move freely in the recording cage with the cables and/or optical fibers attached to the corresponding implants.

Step-down inhibitory avoidance (SDIA) task

The training apparatus consisted of a Plexiglas box (50 x 25 x 25 cm) with a wood platform (5 x 8 x 25 cm) on the left end of a series of bronze bars that made up the floor of the box. Before training, rats were handled for 5 min/day during 5 days (HAN animals) or put on the SDIA training box platform and allowed to freely explore the SDIA training box for 5 min/day during 5 days (PEX animals). One day after the end of these procedures, the animals were placed on the platform facing the left rear corner of the apparatus and, when they stepped down and placed their four paws on the grid, received a 2 s-long 0.8 mA scrambled footshock (training session, TR). Immediately after training, the animals were returned to their home cages and 24 h later placed again on the training box platform for 40 s to reactivate SDIA memory (reactivation session, RA). During these 40 s, the animals explored the platform avoiding stepping down from it. We did not observe any significant behavioral difference between HAN and PEX animals during the reactivation session. Avoidance memory retention was evaluated 1 day after training or reactivation by placing the animals on the training box platform and measuring their latency to step down (test session, TEST). The test session finished when the rats stepped down to the grid (footshock omitted) or after 500 s. Non-treated HAN and PEX animals behaved similarly during the test session. They stayed on the platform in a minimal movement state showing avoidance behavior. Animals were trained and tested only once.

Optogenetic stimulation

For optogenetic experiments, rats were injected with AAV-CAG-ArchT-GFP and implanted with an optic fiber in the MS, as described above. Optic fibers were coupled to blue-light (470 nm) or yellow-light (565 nm) emitting LEDs (ThorLabs). Light delivery was driven using a DC4104 LED driver (ThorLabs). The MS was continuously illuminated during the reactivation session.

Electrical stimulation

FFx stimulation was performed using bipolar electrodes (stainless steel PFA-coated wire, 50-µm diameter) with tips separated vertically 0.5 mm. A voltage/current stimulator (STG4004, Multichannel Systems) was used to generate stimuli. For theta stimulation, single pulses were delivered at 7.7 Hz. For high-frequency stimulation (HFS), single pulses were delivered at 100 Hz. For theta-burst stimulation (TBS) four single-pulse trains at 500 Hz were delivered at 7.7 trains per second (7.7 Hz). Stimulation protocols used 10-50 µA biphasic pulses (pulse width 500 µs). Stimulation intensity was determined in pilot experiments; 10-50 µA was the smallest current range able to induce hPAC with modulation index values similar to those observed in PEX animals during the reactivation session.

In vivo electrophysiology

Electrophysiological signals were acquired using the Cerebus Neural Signal Processor system (Blackrock Microsystems). Signals were amplified, filtered at cut-off frequencies of 0.3 Hz and 250 Hz and sampled at 1 kHz. Data were analyzed offline in MATLAB (RRID: SCR_001622) using built-in and custom written routines (Signal Processing Toolbox). Anatomical localization of the electrodes was identified from LFP features as well as from histological confirmation of the electrodes' tracks, as previously described (Brankack et al., 1993; Bragin et al. 1995). Baseline field potentials were acquired in a familiar recording cage one hour before memory reactivation. We used the first 40 s of stable signals in the recording cage during which the animal was awake and in a minimal movement state with mean velocity < 1 cm/s, similar to the behavior observed during the memory reactivation session. Electrical stimulation using squared pulses can contaminate LFP signals with broadband noise. To minimize this interference, we wrote an algorithm of peak detection using the Signal Processing Toolbox. This algorithm detected artifacts by identifying the local maxima around stimulation times. Since the longest continuous period of stimulation was 8 ms (corresponding to four pulses at 500 Hz), we excluded from further analysis data in a window of ±10 ms around the artifacts detected. Power spectra were computed using the

Welch periodogram method (4 s Hamming windows, 75% overlap). To construct spectrograms, power spectrum was calculated using sliding windows of 4 s and 1 s steps. To avoid spurious comparisons of power values resulting from differences in the absolute raw signal magnitudes, we normalized each power spectrum by the power of the frequency band under 250 Hz computed from the spectrum obtained before memory reactivation. Theta, slow gamma ($_S$gamma) and fast gamma ($_F$gamma) band power were defined as the average power in the frequency range of 5-10 Hz, 35-55 Hz and 65-100 Hz, respectively. To determine the effect of intra-MS MUS infusion on spontaneous hippocampal oscillatory activity, power variation was calculated as post-infusion band power/pre-infusion band power *100, considering 10 min-long intervals. For theta-gamma phase-amplitude cross-frequency coupling analysis, LFP signals were filtered at theta, $_S$gamma and $_F$gamma frequency bands. Theta phase and gamma amplitude were extracted using the Hilbert transform. Theta phase was binned into 18 intervals of 20°. The mean amplitude of gamma bands was computed for each theta phase bin and normalized by the sum of amplitude values over all bins. The modulation index (MI) was computed using an adaptation of the Kullback-Leibler distance between the uniform distribution, and the probability function derived from mean amplitude per phase distribution, as described in Tort el al. (2009). Comodulograms were obtained by expressing the MI of several frequency band pairs (4 Hz bandwidths, 1 Hz steps for phase frequencies; 10 Hz bandwidths, 2 Hz steps for amplitude frequencies) in a bi-dimensional pseudo-color plot (Tort el al., 2009). Mean MIs were obtained by averaging the corresponding MI values in the (5-10 Hz) x (35-55 Hz) or (5-10 Hz) x (65-100 Hz) regions of the comodulograms. To calculate MI we used LFP recordings from the entire 40 s-long reactivation session. Events of $_S$gamma and $_F$gamma amplitude were defined as time intervals when gamma power surpassed by 2.5 sd their respective time-averaged power. These events were identified and then the theta phase associated to each event was determined, as in Colgin et al. (2009). To avoid the analysis of artifactual events, time intervals with power above 6 sd in the computations were discarded. Events separated by less than 100 ms were merged and considered as a single event. Theta phase at the time

points corresponding to the maximum of each gamma event was extracted and the circular mean computed, obtaining a single-phase value associated to the occurrence of high amplitude. The time-course for $_{S}$gamma and $_{F}$gamma events distribution over theta phase was obtained by averaging values in 5 s-long windows. To equalize theta and gamma power between HAN and PEX animals we computed theta, $_{S}$gamma and $_{F}$gamma power in consecutive windows based on their power spectrums (Welch periodogram method, consecutive windows of 1 s in 0.5 s steps), excluded windows with power outside boundaries defined for each group (below 75th percentile for PEX animals and above that percentile for HAN animals) and used the remaining windows to compute MI values. Digital video cameras fixed above the SDIA apparatus were used for tracking animals' position. Video data were acquired at 30 frames/s and analyzed using TopScan system (RRID: SCR_017141). During RA, all animals stayed on the platform in a minimal movement state, thus excluding the possibility that speed-dependent variations in hippocampal LFP activity account for our results.

Immunoblotting

Tissue punches from dorsal CA1 were homogenized in ice-chilled homogenization buffer (10 mM Tris-HCl, pH 7.4, containing 0.32 M sucrose, 1 mM EDTA, 1 mM EGTA, 1 mM PMSF, 10 µg/ml aprotinin, 15 µg/ml leupeptin, 10 µg/ml bacitracin, 10 µg/ml pepstatin, 50 mM NaF, and 1 mM sodium orthovanadate). Protein concentration was determined using the Pierce BCA protein assay kit (Thermo Fisher Scientific). Equal amounts of total protein (15 µg/lane) were resolved on SDS/PAGE (10% gels) under reducing conditions and electro-transferred onto PVDF membranes. Blots were blocked for 2 h in TTBS (100 mM Tris-HCl, 0.9% NaCl, 0.1% Tween 20, pH 7.6), incubated overnight at 4 °C with anti-C/EBPβ (1:20,000; RRID: AB_626772) or anti-Zif268 (1:5,000; RRID: AB_2231020) antibodies, washed with TTBS and incubated with HRP-coupled anti-IgG secondary antibody (1:200,000; RRID: AB_641171 or RRID: AB_641180, respectively). Amersham ECL Prime Western Blotting Detection Reagent (GE Healthcare) was used to detect immunoreactivity. For loading control, blots

were stripped, incubated overnight at 4 °C with anti-GAPDH (1:20,000; RRID: AB_307275) and then incubated with HRP-coupled anti-IgG secondary antibody. Immunoreactivity was detected as described above. Blots were acquired and quantified using Amersham Imager 600 and ImageQuant TL 8.1 analysis software.

Immunofluorescence

Animals were deeply anesthetized with thiopental and transcardially perfused with 4% paraformaldehyde (PFA; pH ~7.2). Brains were removed, placed in PFA at 4 °C overnight, transferred to 30% sucrose, and allowed to settle for 48 h. Brains were cut in 50 µm coronal sections in a cryostat. Free-floating slices from the rostral-caudal extent of the dorsal hippocampus and the medial septum were rinsed with PBS, incubated in PBST (0.2% Triton X-100) for 1 h and blocked for 2 h at room temperature. Slices were incubated with anti-GFP (1:1,000; RRID: AB_300798) overnight at 4 °C and then washed in PBST and incubated with Alexa Fluor 488 anti-chicken (1:1,000; RRID: AB_2534096) for 2 h at room temperature. Slices were counterstained with DAPI (1:1,000; RRID: AB_2629482), mounted with Fluoromount-G and stored at -20 °C until image acquisition. Images were acquired using a Leica DM5000 fluorescence microscope and a CoolSNAP HQ2 CCD Camera in 16-bit grayscale. For visualization, pseudo-colour was applied (linear LUT covered full images, Image-Pro Plus 7.0 software).

Histology

To verify cannula placement, we infused 4% methylene-blue into the MS (0.5 µl) or dorsal CA1 (1 µl) after the end of the behavioral tests. Rats were killed 30 min thereafter and the dye spread was taken as indication of the diffusion of the drug previously injected. Data from animals with incorrect cannula implants (4%) were excluded from statistical analysis. Rats with cannula and electrode implants were deeply anesthetized and transcardially perfused with 4% PFA. Brains were removed, left in 30% sucrose for 48 h and coronal sections were cut with a cryostat (50 µm). Relevant sections were selected and stained with cresyl violet to confirm implant location.

Quantification and statistical analysis

Statistical analyses were performed using GraphPad Prism 8 software (RRID: SCR_002798). Significance was set at $P < 0.05$. Sample size for each experiment is indicated in the figures (dots). No statistical methods were used to determine sample sizes; the number of subjects per group was based on previous reports and experience for each experiment to yield high power to detect specific effects. Subjects were randomly assigned to experimental groups. Training step-down latencies were expressed as mean ± SEM and analyzed using unpaired Student's t-test. Because of the 500 s ceiling imposed, test step-down latencies were expressed as median ± IQR, analyzed by two-tailed Mann-Whitney U test, and Spearman's rank correlation utilized to determine the strength and direction of the putative monotonic association between the mnemonic effect of post-reactivation manipulations and hippocampal oscillatory activity during recall. Immunoblots and electrophysiological data were expressed as mean ± SEM and analyzed using one-sample t test with theoretical mean = 100, paired t-test, unpaired Student's t-test, one-way repeated-measures ANOVA or two-way ANOVA followed by Bonferroni's multiple comparisons test, Rayleigh test or Watson-Williams multi-sample test, as appropriate.

Results

Hippocampus-dependent avoidance memory reconsolidation requires prior learning of related non-aversive information and is accompanied by increased theta-gamma phase-amplitude coupling.

To analyze whether hPAC and avoidance memory reconsolidation are causally related, we trained adult male Wistar rats (3-month-old; 300-350 g) in a one-trial, step-down, inhibitory avoidance learning paradigm (SDIA), which generates a long-lasting fear-motivated avoidance memory (Bernabeu et al., 1995; Cammarota et al., 2000; Bekinschtein et al., 2007). SDIA memory reconsolidation engages the hippocampus only when animals acquired the avoidance response in an environment they previously considered safe (Radiske at al., 2017). Therefore, to differentiate reconsolidation-specific mechanisms from those related

merely to memory recall, rats were handled (HAN group) or allowed to explore the SDIA training box freely during 5 minutes once daily for 5 days (PEX group). This last procedure induces learning of non-aversive SDIA-related information without affecting SDIA memory acquisition, strength or persistence, and renders SDIA memory susceptible to hippocampus-dependent reconsolidation upon non-reinforced reactivation (Radiske et al., 2017). Twenty-four hours later, the animals were trained in SDIA (0.8 mA/2 s footshock) and one day thereafter submitted to a 40 s-long non-reinforced memory reactivation session (RA) able to induce reconsolidation but not extinction of the learned avoidance response (Cammarota et al., 2004; Radiske et al., 2017). Protein synthesis dependency is a reconsolidation hallmark, and CCAAT/enhancer-binding protein β (C/EBPβ) is part of the molecular signature of this process (Milekic et al., 2007). In fact, it has been suggested that aversive memories resistant to post-retrieval hippocampal protein synthesis inhibition are also immune to hippocampal C/EBPβ signaling disruption (Taubenfeld et al., 2001). In agreement with this suggestion, we found that intra-dorsal CA1 infusion of C/EBPβ antisense oligonucleotides (C/EBPβ-ASO), at a dose that reduced basal C/EBPβ levels ~30% (Fig. 1A; C/EBPβ: $t(4) = 8.499$, $P = 0.0011$ in one-sample t test, theoretical mean = 100), or of the protein synthesis inhibitor anisomycin (ANI), 5 min but not 6 h after RA, triggered amnesia in PEX but not in HAN animals (Fig. 1B; PEX 5': $U = 7.500$, $P = 0.0017$ for VEH vs ANI; $U = 12.50$, $P = 0.0093$ for sASO vs ASO in Mann Whitney test). Accordingly, memory reactivation increased dorsal CA1 C/EBPβ levels only in PEX animals (Fig. 1C; $F(1, 8) = 17.73$, $P = 0.0030$ for interaction; $F(1, 8) = 3.795$, $P = 0.0872$ for pre-exposition effect; $F(1, 8) = 21.46$, $P = 0.0017$ for reactivation effect in two-way ANOVA. $P < 0.001$ for PEX RA vs PEX NR in Bonferroni's multiple comparisons test). Confirming and extending previous findings, analysis of dorsal CA1 LFP during RA showed that slow gamma ($_S$gamma; 35-55 Hz) power augmented in HAN and PEX animals, but theta and fast gamma ($_F$gamma; 65-100 Hz) power increased only in PEX rats (Fig. 1D; HAN $_S$gamma power: $t(5) = 2.838$, $P = 0.0363$; PEX theta power: $t(5) = 2.709$, $P = 0.0423$; PEX $_S$gamma power: $t(5) = 2.628$, $P = 0.0466$; PEX $_F$gamma power: $t(5) = 3.735$, $P = 0.0135$ for Before vs During RA in paired t test). hPAC was stronger in PEX than in HAN animals and

independent of theta fluctuation (Fig. 1E-F; theta-$_S$gamma MI: t(10) = 4.340, P = 0.0015; theta-$_F$gamma MI: t(10) = 4.342, P = 0.0015 for HAN vs PEX in unpaired t test). The number of gamma events, defined as periods when power of the gamma frequency sub-bands exceeded 2.5 sd, did not differ between HAN and PEX animals during RA (Fig. 1G), but $_S$gamma and $_F$gamma events occurred preferentially around the peak of the theta cycle throughout the reactivation session only in PEX animals (Fig. 1H; $_S$gamma events: Z = 26.11, P < 0.0001; $_F$gamma events: Z = 27.62, P < 0.0001 in Rayleigh test). The difference in coupling strength between PEX and HAN animals persisted even after equalizing theta, $_S$gamma or $_F$gamma power (Fig. 1I; equalized theta power: theta-$_S$gamma MI: t(10) = 6.085, P = 0.0001; theta-$_F$gamma MI: t(10) = 3.231, P = 0.0090; equalized $_S$gamma power: theta-$_S$gamma MI: t(10) = 8.945, P < 0.0001; theta-$_F$gamma MI: t(10) = 2.969, P = 0.0141; equalized $_F$gamma power: theta-$_S$gamma MI: t(10) = 4.874, P = 0.0006; theta-$_F$gamma MI: t(10) = 2.631, P = 0.0251 for HAN vs PEX in unpaired t test), indicating that it did not result from power increase or improved phase detection, and suggesting that hPAC, but not theta or gamma activity per se, is associated with memory reconsolidation. In agreement with this assertion, theta-$_S$gamma MI and theta-$_F$gamma MI, but not theta, $_S$gamma or $_F$gamma power, correlated negatively with memory retention in PEX animals that received ANI in dorsal CA1 5 min after RA (Fig 1J).

Medial septum inactivation impedes hippocampal theta-gamma phase-amplitude coupling and the amnesia caused by post-retrieval hippocampal protein synthesis inhibition and C/EBPβ knockdown.

Medial septum (MS) inactivation reduces hippocampal theta rhythm, and it has been repeatedly used to analyze the involvement of hPAC in memory processing and behavior (Winson, 1978; Shirvalkar, et al., 2010; Brandon et al., 2014). In our preparation, intra-MS infusion of the GABAA agonist muscimol (MUS; 0.2 μg/side) diminished theta oscillations in dorsal CA1 for at least 3 hours without affecting gamma activity (Fig. 2A, Top panel; theta power variation: F(1.929, 5.789) = 12.47, P = 0.0082 in RM one-way ANOVA. *P < 0.05, **P

< 0.01 in Bonferroni's multiple comparisons test) or SDIA memory retrieval (Fig. 2A, Bottom panel). By itself, intra-MS MUS infusion before memory reactivation had no effect on SDIA memory retention, regardless of pre-training behavioral manipulations, but cancelled the amnesia triggered by the post-reactivation intra-CA1 administration of ANI and C/EBPβ-ASO (Fig. 2B; PEX: U = 8.000, P = 0.0079 for VEH+VEH vs VEH+ANI; U = 12.00, P = 0.0275 for VEH+sASO vs VEH+ASO in Mann Whitney test), and impeded the reactivation-induced increase in C/EBPβ levels (Fig. 2C; t(8) = 3.589, P = 0.0071 for VEH vs MUS in unpaired t test). In PEX animals, MS inactivation decreased theta, but not slow gamma and fast gamma power (Fig. 2D; theta power: HAN/MUS, t(4) = 3.9530, P = 0.0168; PEX/VEH, t(4) = 3.277, P = 0.0306; PEX/MUS, t(4) = 9.836, P = 0.0006. $_{S}$gamma power: HAN/VEH, t(4) = 3.721, P = 0.0205; HAN/MUS, t(4) = 6.153, P = 0.0035; PEX/VEH, t(4) = 3.586, P = 0.0230; PEX/MUS, t(4) = 3.317, P = 0.0295. $_{F}$gamma power: PEX/VEH, t(4) = 4.662, P = 0.0096; PEX/MUS, t(4) = 2.850, P = 0.0464 for Before RA vs During RA in paired t test) and diminished the strong nested theta-gamma activity induced by SDIA memory reactivation (Fig. 2E; theta-$_{S}$gamma MI: F(1,16) = 12.09, P = 0.0031 for interaction; F(1,16) = 17.09, P = 0.0008 for pre-exposition effect; F(1,16) = 33.87, P < 0.0001 for treatment effect; theta-$_{F}$gamma MI: F(1,16) = 10.37, P = 0.0053 for interaction; F(1,16) = 19.56, P = 0.0004 for pre-exposition effect; F(1,16) = 16.22, P = 0.0010 for treatment effect in two-way ANOVA. P < 0.001 for HAN/VEH vs PEX/VEH, HAN/MUS vs PEX/VEH, or PEX/VEH vs PEX/MUS in Bonferroni's multiple comparisons test).

Optogenetic silencing of the medial septum during recall impedes avoidance memory destabilization.

Our results corroborate and expand previous findings suggesting that increased hippocampal theta-gamma phase-amplitude coupling is functionally linked to memory reconsolidation, and support the hypothesis that this interaction is necessary for SDIA memory destabilization during recall. However, in our preparation, the inhibitory effect of intra-MS MUS administration on hippocampal oscillatory activity extended well beyond the

end of the reactivation session, making it difficult to link reactivation-induced hippocampal rhythms and memory destabilization irrefutably. To overcome this drawback, and limit MS inactivation to the duration of the reactivation session, we virally expressed yellow light-sensing archaerhodopsin T (ArchT) in the MS of PEX animals to optogenetically silence this brain region. One day after the last pre-exposition session, PEX animals were trained in SDIA and one day later submitted to a memory reactivation session. During that session, one group of animals was used as non-stimulated control, while other two groups were optically stimulated in the MS with blue light (470 nm) or yellow light (565 nm). Because ArchT responds to green-yellow light but not to blue light, stimulation at 470 nm was used as an additional control. Five minutes after memory reactivation, animals received bilateral intra-CA1 infusions of VEH or ANI and retention was tested one day later. As expected, ANI caused SDIA amnesia in non-stimulated PEX animals as well as in PEX animals stimulated with blue light in the MS. Yellow light stimulation had no effect on SDIA memory retention, but hindered the amnesic effect of ANI and reduced hPAC (Fig. 3A; Light OFF: $U = 10.00$, $P = 0.0046$; Blue ON: $U = 13.00$, $P = 0.0093$ for VEH vs ANI in Mann-Whitney test), as well as theta power in the hippocampus (Fig. 3B; $F(1.658, 8.291) = 21.30$, $P = 0.0007$ in RM one-way ANOVA. *$P < 0.05$, **$P < 0.01$ in Bonferroni's multiple comparisons test). MS stimulation with yellow light did not alter hippocampal gamma oscillations (Fig. 3B).

Induction of artificial hippocampal theta-gamma phase-amplitude coupling during recall restores the amnesic effect of reconsolidation blockers in medial septum-inactivated animals.

Our analyses demonstrate that the difference in hPAC strength between HAN and PEX animals does not result from increased oscillatory power or enhanced phase identification, but reflects an active memory process instead. However, the steep decline in theta activity produced by MS inactivation prevented us from decisively determining the existence of a causal connection between hPAC and memory destabilization. To get around this problem, we took advantage of the fact that the MS projects to the hippocampus through the fimbria-

fornix (FFx; Manseau et al., 2008; Müller and Remy, 2018), and it is known that electrical stimulation of this pathway can restore hippocampal theta rhythm and hPAC in MS-lesioned animals (Yoder and Pang, 2005; McNaughton et al., 2006) without affecting gamma activity (Shirvalkar et al., 2010). We found that FFx theta stimulation and FFx theta-burst stimulation (TBS), but not FFx high-frequency stimulation (100 Hz), bypassed MUS-induced MS inactivation and promoted theta activity in dorsal CA1 (Fig. 4A). However, only FFx TBS nested hippocampal gamma activity within theta envelopes (Fig. 4B; theta-$_S$gamma MI: $t(4) = 4.443$, $P = 0.0113$; theta-$_F$gamma MI: $t(4) = 5.384$, $P = 0.0058$ for Before vs During FFx TBS in paired t test) and restored the amnesia provoked by the post-reactivation intra-CA1 administration of ANI in PEX animals. This effect was seen only when FFx TBS was applied during RA, but not 5 min thereafter or in its absence, suggesting that it was contingent on memory reactivation. TBS delivered in the corpus callosum, 1 mm above the FFx, did not re-establish the capacity of ANI to induce amnesia (Fig. 4C-D; RA: $U = 9.00$, $P = 0.0009$; RA$_{(LFP)}$: $U = 10.00$, $P = 0.0046$ for VEH vs ANI in Mann-Whitney test; theta-$_S$gamma MI: $t(8) = 3.670$, $P = 0.0063$; theta-$_F$gamma MI: $t(8) = 4.419$, $P = 0.0022$ for Before RA vs During RA in paired t test). Notably, theta-$_S$gamma MI and theta-$_F$gamma MI, but not theta, $_S$gamma or $_F$gamma power, correlated with the amnesic effect of ANI (Fig 4D). We also found that FFx TBS renewed the amnesic effect of post-RA intra-CA1 C/EBPβ-ASO infusions in PEX animals that received intra-MS MUS 15 min before memory reactivation (Fig. 4E; TBS: $U = 7.00$ and $P = 0.0012$ for sASO vs ASO in Mann Whitney test).

Induction of artificial theta-gamma phase-amplitude coupling during recall makes reconsolidation-resistant memory vulnerable to reactivation-dependent amnesia.

We next investigated the effect of FFx TBS in rats resistant to hippocampus-dependent reconsolidation. We reasoned that if hPAC were indeed necessary for memory destabilization, then perhaps increasing hPAC artificially during recall could help destabilize SDIA memory in HAN animals, making it vulnerable to post-reactivation amnesic manipulations. To test this hypothesis, HAN animals were trained in SDIA and one day later

447 submitted to a reactivation session during which they received TBS in FFx to induce artificial
448 hPAC. Five minutes after memory reactivation, rats received bilateral intra-dorsal CA1
449 injections of VEH or ANI, and retention was evaluated one day later. As expected,
450 unstimulated HAN animals given VEH or ANI retained the learned avoidance response.
451 However, memory became susceptible to ANI in animals that received FFx TBS during
452 reactivation. FFx TBS did not make memory vulnerable to ANI when delivered immediately
453 after the reactivation session or in its absence (Fig. 5A; RA: $U = 11.00$, $P = 0.0041$; $RA_{(LFP)}$:
454 $U = 15.00$, $P = 0.0167$ for VEH vs ANI in Mann-Whitney test). The amnesic potency of ANI
455 correlated with the strength of artificially-induced hPAC, but not with theta, $_{S}$gamma or
456 $_{F}$gamma power at reactivation (Fig. 5A). FFx TBS also enabled RA-dependent SDIA
457 amnesia in HAN animals that received intra-dorsal CA1 C/EBPβ-ASO, but not C/EBPβ-
458 sASO, 5 min after RA (Fig. 5B; TBS, $U = 4.000$, $P = 0.0047$ for sASO vs ASO in Mann-
459 Whitney test).
460
461 **Discussion**
462 Our data confirm that hPAC increases during avoidance memory reactivation only when this
463 process induces hippocampus-dependent reconsolidation (Radiske et al., 2017), and show
464 that this theta-gamma interaction, but not theta or gamma activity per se, is causally linked to
465 destabilization of the avoidance response. Importantly, our results also demonstrate that
466 artificial hPAC generation during recall can destabilize memories that are normally resistant
467 to reconsolidation, making them liable to reactivation-targeted amnesic manipulations.
468 SDIA memory reactivation enables hippocampus-dependent reconsolidation only when it
469 results in conflicting representations about the possible consequences of avoidance. Then, it
470 is tempting to speculate that hPAC reflects the switch between aversive and non-aversive
471 states that probably underlies the decision-making process that PEX animals undergo during
472 the reactivation session. This hypothesis is in agreement with findings showing that hPAC
473 increases for both error and correct trials during associative learning (Tort et al., 2009) and is

correlated with state-dependent information processing during decision-making (Amemiya and Redish, 2018).

In view of the fact that network activity modulation is intertwined with long-term plasticity, and the onset of reconsolidation is linked to changes in synaptic weight driven by reversible adjustments in AMPAR function (Hong et al., 2013), the increased hPAC observed in PEX animals may reflect modifications in hippocampal synaptic efficacy. In fact, the pattern of oscillatory activity in the hippocampus of PEX rats during memory reactivation resembles that necessary for induction of long-term potentiation (LTP) in dorsal CA1 (Thomas et al., 1998). Potentiated synapses may return to a protein synthesis-dependent state following LTP reactivation and, when multiple inputs converge, the active synapses must compete for plasticity factors to stay potentiated (Fonseca et al., 2004; 2006). We propose that a similar mechanism is triggered when antagonistic representations clash over the control of behavior at recall, with the dominant trace becoming destabilized, as previously suggested (Eisenberg et al., 2003). Since FFx-TBS may induce LTP in CA1 (Li et al., 2005), such a mechanism could explain why artificial hPAC circumvented the inhibitory effect of MS inactivation on memory destabilization and made animals naturally resistant to reconsolidation become sensitive to post-reactivation amnesia only when generated concomitantly with avoidance memory recall.

Targeting memory reconsolidation is a promising therapeutic approach to treat PTSD that offers the opportunity to erase intrusive recollections in a single session (Nader et al., 2013). However, recall does not always induce destabilization of the reactivated trace, which limits its translational value. Our findings have important implications for the implementation of reconsolidation-based therapies in clinical practice. They not only show that hPAC strength can be used as an estimator of memory destabilization, which could help optimize memory reactivation protocols and adjust pharmacological interventions to suit the needs of individual patients, but also indicate that it is feasible to overcome the constraints on reconsolidation through brain stimulation protocols similar to those employed to alleviate motor and cognitive dysfunctions (Hao et al., 2005; Laxton et al., 2010; Lyons et al., 2011). This could be useful

to treat patients refractory to conventional therapies, or when the source of the trauma is unknown. However, it is important to note that the nature of conflicting signals at recall can differ among avoidance memory types. Therefore, our results should not be generalized to conclude that hPAC is involved in the destabilization of all avoidance memories. For example, while hippocampus-dependent SDIA reconsolidation is linked to reactivation of contradictory representations regarding the possible consequences of avoidance (Radiske et al., 2017), induction of step-through avoidance (STA) memory reconsolidation involves competition between innate and learned responses, and requires protein synthesis and C/EBPβ expression in the amygdala instead of the hippocampus (Taubenfeld et al., 2001; Milekic et al., 2007). Given that similar molecular mechanisms underlie hippocampus-dependent and amygdala-dependent avoidance reconsolidation, and switches between fear and safety states engage distinct theta-gamma coupling patterns in the basolateral amygdala (Stujenske et al., 2014), it would be interesting to evaluate whether reactivation-induced theta-gamma interactions in the amygdala are associated with STA memory destabilization.

References

Amemiya S, Redish AD (2018) Hippocampal Theta-Gamma Coupling Reflects State-Dependent Information Processing in Decision Making. Cell Rep. 25:3894–3897.

Batelaan NM, Bosman RC, Muntingh A, Scholten WD, Huijbregts KM, van Balkom AJLM (2017) Risk of relapse after antidepressant discontinuation in anxiety disorders, obsessive-compulsive disorder, and post-traumatic stress disorder: systematic review and meta-analysis of relapse prevention trials. BMJ 358:j3927.

Bernabeu R, Izquierdo I, Cammarota M, Jerusalinsky D, Medina JH (1995) Learning-specific, time-dependent increase in [3 H] phorbol dibutyrate binding to protein kinase C in selected regions of the rat brain. Brain Res. 685:163–168.

Bekinschtein P, Cammarota M, Igaz LM, Bevilaqua LR, Izquierdo I, Medina JH (2007) Persistence of long-term memory storage requires a late protein synthesis- and BDNF-dependent phase in the hippocampus. Neuron 53:261-77.

Bos MG, Beckers T, Kindt M (2014) Noradrenergic Blockade of Memory Reconsolidation: A Failure to Reduce Conditioned Fear Responding. Front. Behav. Neurosci. 8:412.

Bragin A, Jandó G, Nádasdy Z, Hetke J, Wise K, Buzsáki G (1995) Gamma (40-100 Hz) oscillation in the hippocampus of the behaving rat. J Neurosci 15:47-60.

Brandon MP, Koenig J, Leutgeb JK, Leutgeb S (2014) New and distinct hippocampal place codes are generated in a new environment during septal inactivation. Neuron 21:789–96.

Brankack J, Stewart M, Fox SE (1993) Current source density analysis of the hippocampal theta rhythm: associated sustained potentials and candidate synaptic generators. Brain Res 615:310-27.

Bryant RA (2019) Post-traumatic stress disorder: a state-of-the-art review of evidence and challenges. World Psychiatry 18:259–269.

Buzsáki G (2002) Theta oscillations in the hippocampus. Neuron 33:325–40.

Buzsáki G (2006) Rhythms of the Brain. Oxford University Press.

Cammarota M, Bevilaqua LR, Ardenghi P, Paratcha G, Levi de Stein M, Izquierdo I, Medina JH (2000) Learning-associated activation of nuclear MAPK, CREB and Elk-1, along with Fos

557 production, in the rat hippocampus after a one-trial avoidance learning: abolition by NMDA
558 receptor blockade. Brain. Res. Mol. Brain. Res. 76:36–46.
559
560 Cammarota M, Bevilaqua LR, Medina JH, Izquierdo I (2004) Retrieval does not induce
561 reconsolidation of inhibitory avoidance memory. Learn. Mem. 11:572–578.
562
563 Colgin LL, Denninger T, Fyhn M, Hafting T, Bonnevie T, Jensen O, Moser MB, Moser EI
564 (2009) Frequency of gamma oscillations routes flow of information in the hippocampus.
565 Nature 462:353–357.
566
567 Dudai Y (2004) The neurobiology of consolidations, or, how stable is the engram? Annu.
568 Rev. Psychol. 55:51–86.
569
570 Dunbar AB, Taylor JR (2017) Reconsolidation and psychopathology: Moving towards
571 reconsolidation-based treatments. Neurobiol. Learn. Mem. 142:162–171.
572
573 Eisenberg M, Kobilo T, Berman DE, Dudai Y (2003) Stability of retrieved memory: inverse
574 correlation with trace dominance. Science 22:1102–4.
575
576 Elsey JWB, Kindt M (2017) Tackling maladaptive memories through reconsolidation: From
577 neural to clinical science. Neurobiol. Learn. Mem. 142:108–117.
578
579 Fonseca R, Nägerl UV, Morris RG, Bonhoeffer T (2004) Competing for memory:
580 hippocampal LTP under regimes of reduced protein synthesis. Neuron 16:1011–20.
581
582 Fonseca R, Nägerl UV, Bonhoeffer T (2006) Neuronal activity determines the protein
583 synthesis dependence of long-term potentiation. Nat. Neurosci. 9:478–80.
584

585 Friedman MJ, Bernardy NC (2017) Considering future pharmacotherapy for PTSD. Neurosci.
586 Lett. 649:181–185.
587
588 Hao S, Tang B, Wu Z, Ure K, Sun Y, Tao H, Gao Y, Patel AJ, Curry DJ, Samaco RC, Zoghbi
589 HY, Tang J (2015). Forniceal deep brain stimulation rescues hippocampal memory in Rett
590 syndrome mice. Nature 15:430–4.
591
592 Haubrich J, Nader K (2018) Memory Reconsolidation. Curr. Top. Behav. Neurosci. 37:151–
593 176.
594
595 Hong I, Kim J, Kim J, Lee S, Ko HG, Nader K, Kaang BK, Tsien RW, Choi S (2013) AMPA
596 receptor exchange underlies transient memory destabilization on retrieval. Proc. Natl. Acad.
597 Sci. USA 14:8218–8223.
598
599 Jensen O, Colgin LL (2007) Cross-frequency coupling between neuronal oscillations. Trends
600 Cognit. Sci. 11:267–269.
601
602 Laxton AW, Tang-Wai DF, McAndrews MP, Zumsteg D, Wennberg R, Keren R, Wherrett J,
603 Naglie G, Hamani C, Smith GS, Lozano AM (2010) A phase I trial of deep brain stimulation
604 of memory circuits in Alzheimer's disease. Ann. Neurol. 68:521–534.
605
606 Li C, Maier DL, Cross B, Doherty JJ, Christian EP (2005) Fimbria-fornix lesions compromise
607 the induction of long-term potentiation at the Schaffer collateral-CA1 synapse in the rat in
608 vivo. J. Neurophysiol. 93:3001–6.
609
610 Lisman JE, Buzsáki G (2008) A neural coding scheme formed by the combined function of
611 gamma and theta oscillations. Schizophr. Bull. 34:974–80.
612

613 Lisman JE, Jensen O (2013) The θ-γ neural code. Neuron 77:1002-16.

614

615 Lisman JE, Talamini LM, Raffone A (2005) Recall of memory sequences by interaction of the
616 dentate and CA3: A revised model of the phase precession. Neural Netw. 18: 1191–201.

617

618 Lyons MK (2011). Deep brain stimulation: current and future clinical applications. Mayo. Clin.
619 Proc. 86:662–72.

620

621 Manseau F, Goutagny R, Danik M, Williams S (2008) The hippocamposeptal pathway
622 generates rhythmic firing of GABAergic neurons in the medial septum and diagonal bands:
623 an investigation using a complete septohippocampal preparation in vitro. J. Neurosci.
624 9:4096–107.

625

626 McGaugh JL (1966) Time-dependent processes in memory storage. Science 153:1351–
627 1358.

628

629 McNaughton N, Ruan M, Woodnorth MA (2006) Restoring theta-like rhythmicity in rats
630 restores initial learning in the Morris water maze. Hippocampus 16:1102–10.

631

632 Merlo E, Milton AL, Goozée ZY, Theobald DE, Everitt BJ (2014) Reconsolidation and
633 extinction are dissociable and mutually exclusive processes: behavioral and molecular
634 evidence. J. Neurosci. 34:2422–31.

635

636 Milekic MH, Pollonini G, Alberini CM (2007) Temporal requirement of C/EBPbeta in the
637 amygdala following reactivation but not acquisition of inhibitory avoidance. Learn. Mem.
638 14:504–11.

639

640 Müller C, Remy S (2018) Septo-hippocampal interaction. Cell. Tissue. Res. 373:565–575.

641

642 Nader K, Schafe GE, Le Doux JE (2000) Fear memories require protein synthesis in the
643 amygdala for reconsolidation after retrieval. Nature 406:722–726.

644

645 Nader K, Hardt O (2009) A single standard for memory: the case for reconsolidation. Nat.
646 Rev. Neurosci. 10:224–34.

647

648 Nader K, Einarsson EO (2010) Memory reconsolidation: an update. Ann. N. Y. Acad. Sci.
649 1191:27–41.

650

651 Nader K, Hardt O, Lanius R (2013) Memory as a new therapeutic target. Dialogues Clin.
652 Neurosci. 15:475–86.

653

654 Polak AR, Witteveen AB, Visser RS, Opmeer BC, Vulink N, Figee M, Denys D, Olff M (2012)
655 Comparison of the effectiveness of trauma-focused cognitive behavioral therapy and
656 paroxetine treatment in PTSD patients: design of a randomized controlled trial. BMC
657 Psychiatry 12:166.

658

659 Pratchett LC, Daly K, Bierer LM, Yehuda R (2011) New approaches to combining
660 pharmacotherapy and psychotherapy for posttraumatic stress disorder. Expert. Opin.
661 Pharmacother. 12:2339–54.

662

663 Przybyslawski J, Sara SJ (1997) Reconsolidation of memory after its reactivation. Behav.
664 Brain. Res. 84:241–246.

665

666 Radiske A, Gonzalez MC, Conde-Ocazionez SA, Feitosa A, Köhler CA, Bevilaqua LR,
667 Cammarota M (2017) Prior learning of relevant nonaversive information is a boundary

condition for avoidance memory reconsolidation in the rat hippocampus. J. Neurosci. 37:9675–9685.

Schwabe L, Nader K & Pruessner JC (2014) Reconsolidation of human memory: brain mechanisms and clinical relevance. Biol. Psychiatry 76:274–80.

Sevenster D, Beckers T, Kindt M (2012) Retrieval per se is not sufficient to trigger reconsolidation of human fear memory. Neurobiol. Learn. Mem. 97:338–45.

Shirvalkar PR, Rapp PR, Shapiro ML (2010) Bidirectional changes to hippocampal theta-gamma comodulation predict memory for recent spatial episodes. Proc. Natl. Acad. Sci. USA 107:7054–9.

Skaggs WE, McNaughton BL, Wilson MA, Barnes CA (1996) Theta phase precession in hippocampal neuronal populations and the compression of temporal sequences. Hippocampus 6:149–173.

Spear N (1973) Retrieval of memory in animals. Psychol. Rev. 80:163–194.

Stujenske JM, Likhtik E, Topiwala MA, Gordon JA (2014) Fear and safety engage competing patterns of theta–gamma coupling in the basolateral amygdala. Neuron 83:919–933.

Taubenfeld SM, Milekic MH, Monti B, Alberini CM (2001) The consolidation of new but not reactivated memory requires hippocampal C/EBPbeta. Nat. Neurosci. 4:813–8.

Thomas MJ, Watabe AM, Moody TD, Makhinson M, O'Dell TJ (1998) Postsynaptic complex spike bursting enables the induction of LTP by theta frequency synaptic stimulation. J. Neurosci. 15:7118–26.

Thome J, Koppe G, Hauschild S, Liebke L, Schmahl C, Lis S, Bohus M (2016) Modification of fear memory by pharmacological and behavioural interventions during reconsolidation. PLoS One 11:e0161044.

Tort AB, Komorowski RW, Manns JR, Kopell NJ & Eichenbaum H (2009) Theta-gamma coupling increases during the learning of item-context associations. Proc. Natl. Acad. Sci. USA 106:20942–7.

Waits WM, Hoge CW (2018) Reconsolidation of Traumatic Memories Using Psychotherapy. Am. J. Psychiatry 175:1145.

Winson J (1978) Loss of hippocampal theta rhythm results in spatial memory deficit in the rat. Science 201:160-3.

Yang Y, Jie J, Li J, Chen W, Zheng X (2019) A novel method to trigger the reconsolidation of fear memory. Behav. Res. Ther. 122:103461.

Yoder RM, Pang KC (2005) Involvement of GABAergic and cholinergic medial septal neurons in hippocampal theta rhythm. Hippocampus 15:381–92.

Legends

Figure 1. *Prior non-aversive learning is a boundary condition for hippocampus-dependent avoidance memory reconsolidation.* ***A,*** Naïve rats received vehicle (VEH; 0.9% saline) in the dorsal CA1 region of one hemisphere and C/EBPβ-ASO (ASO; 2 nmol/μl) in the other. Ninety minutes later, the animals were decapitated and the dorsal CA1 region dissected out and homogenized to determine C/EBPβ, Zif268 and GAPDH protein levels by immunoblotting (n = 5 per group). ***B,*** Rats were handled (HAN animals) or allowed to freely

explore the step-down inhibitory avoidance (SDIA) training box (PEX animals) during 5 min once daily for 5 consecutive days. Twenty-four hours after the last handling or pre-exposition session, the animals were trained in SDIA (0.8 mA/2 s) and one day later submitted to a 40 s-long non-reinforced memory reactivation session (RA). Five minutes or 6 h after RA the animals received bilateral intra-dorsal CA1 infusions of VEH, anisomycin (ANI; 160 µg/side), C/EBPβ antisense oligonucleotides (ASO; 2 nmol/µl), or scrambled ASO (sASO; 2 nmol/µl). Retention was evaluated 1 day later (TEST; n = 8-9 per group). ***C,*** HAN and PEX animals were trained as in B, but 24 h after training were handled during 40 s (NR) or submitted to RA, killed by decapitation 90 min thereafter and the dorsal CA1 region dissected out and homogenized to determine C/EBPβ and GAPDH protein levels by immunoblotting (n = 5 per group). ***D,*** Representative raw hippocampal LFP traces and power spectrum density plots for HAN and PEX animals for theta (θ; 5-10 Hz), $_S$gamma (γ_S; 35-55 Hz) and $_F$gamma (γ_F; 65-100 Hz) frequency bands showing reactivation-induced alterations in hippocampal oscillatory activity (n = 6 per group). ***E,*** Mean theta-$_S$gamma and theta-$_F$gamma modulation index (MI) and representative phase-amplitude comodulograms for HAN and PEX animals during RA. ***F,*** MI and theta power computed in 8 non-overlapping blocks throughout RA for PEX animals. ***G,*** Mean number of $_S$gamma and $_F$gamma events for HAN and PEX animals during RA. ***H,*** Gamma events distribution over theta phase for HAN and PEX animals during RA. 0°= theta peak. ***I,*** MIs calculated using epochs with equalized theta, $_S$gamma or $_F$gamma power (expressed as $\mu V^2/Hz$) for HAN and PEX animals during RA. ***J,*** SDIA-trained PEX animals with cannulas and electrode arrays implanted in the CA1 region of the dorsal hippocampus were submitted to RA, during which LFP signals were recorded. Five minutes after RA the animals received VEH or ANI into dorsal CA1. Retention was evaluated 1 day later (median = 500, IQR = 379-500 for VEH; median = 78, IQR = 25-235 for ANI; U = 4.00, P = 0.0004 for VEH vs ANI in Mann Whitney test; n = 9 per group). Bar plots represent Spearman's r correlation coefficient between test latency and normalized theta power (θ_{Power}; mean = 0.373, SEM = 0.026), $_S$gamma power ($\gamma_{S\ Power}$; mean = 0.087, SEM = 0.007),

751 $_{F}$gamma power ($\gamma_{F\ Power}$; mean = 0.029, SEM = 0.003), theta-$_{S}$gamma MI ($\gamma_{S\ MI}$; mean =
752 $0.479x10^{-3}$, SEM = $0.008x10^{-3}$) or theta-$_{F}$gamma MI ($\gamma_{F\ MI}$; mean = $0.728x10^{-3}$, SEM =
753 $0.156x10^{-3}$) during RA for animals that received ANI. Data expressed as median ± IQR or
754 mean ± SEM. *p<0.05, **p<0.01, ***p<0.001.
755
756 **Figure 2.** *Medial septum inactivation during avoidance memory reactivation impedes*
757 *hippocampal theta-gamma phase-amplitude coupling and memory destabilization.* ***A,*** T*op*
758 *panel:* Representative raw hippocampal LFP traces at baseline and 20 min post-infusion
759 from animals given muscimol (MUS; 0.2 µg/µl) into the medial septum (MS). *Middle panel:*
760 Theta (θ; 5-10 Hz), $_{S}$gamma (γ_S; 35-55 Hz) and $_{F}$gamma (γ_F; 65-100 Hz) power variation from
761 baseline (B) at different time points after intra-MS MUS infusion (n = 4). *Bottom panel:* Rats
762 were handled (HAN animals) or allowed to freely explore the step-down inhibitory avoidance
763 (SDIA) training box (PEX animals) during 5 min once daily for 5 consecutive days. Twenty-
764 four hours after the last handling or pre-exposition session, animals were trained in SDIA
765 (0.8 mA/2 s). One day later, they received injections of vehicle (VEH; 0.9% saline) or MUS
766 into MS and 15 min thereafter were submitted to a retention test session (n = 8 per group).
767 **B,** One day after training, HAN and PEX animals received VEH or MUS into MS and 15 min
768 thereafter were submitted to a 40 s-long non-reinforced memory reactivation session (RA).
769 Five minutes after RA, the animals received bilateral intra-dorsal CA1 infusions of VEH,
770 anisomycin (ANI; 160 µg/side), C/EBPβ antisense oligonucleotides (ASO; 2 nmol/µl), or
771 scrambled ASO (sASO; 2 nmol/µl). Retention was evaluated 1 day later (TEST; n = 8-9 per
772 group). ***C,*** PEX animals were treated as in B, but 90 min after RA were killed by decapitation
773 and the dorsal CA1 region dissected out and homogenized to determine C/EBPβ and
774 GAPDH protein levels by immunoblotting (n = 5 per group). ***D,*** Normalized theta (θ),
775 $_{S}$gamma (γ_S) and $_{F}$gamma (γ_F) power before and during RA for HAN and PEX animals that
776 received intra-MS VEH or MUS 15 min before RA (n = 5 per group). ***E,*** Mean theta-$_{S}$gamma
777 and theta-$_{F}$gamma modulation index (MI) and representative phase-amplitude

778 comodulograms for HAN and PEX animals during RA. Data expressed as median ± IQR or
779 mean ± SEM. *p<0.05, **p<0.01, ***p<0.001. #p < 0.05 in one-sample Student's t-test with
780 theoretical mean = 100.
781
782 **Figure 3.** *Medial septum optogenetic silencing impedes memory destabilization.* ***A,*** Top
783 panel: Rats expressing archaerhodopsin T in the medial septum (MS) were allowed to freely
784 explore the step-down inhibitory avoidance (SDIA) training box during 5 min once daily for 5
785 consecutive days (PEX animals) and 24 h after the last pre-exposition session were trained
786 in SDIA (TR; 0.8 mA/2 s). One day post-TR, animals were submitted to a 40 s-long non-
787 reinforced memory reactivation session (RA) during which the MS was not stimulated (Light
788 OFF) or optogenetically stimulated with blue light (470 nm; Blue ON) or yellow light (565 nm;
789 Yellow ON). Five min after RA, rats received bilateral injections of vehicle (VEH; 0.9%
790 saline) or anisomycin (ANI; 160 µg/side) in dorsal CA1. Retention was evaluated 1 day later
791 (TEST; n = 9-10 per group). Bottom panel: Representative phase-amplitude comodulograms
792 during RA for each experimental group. ***B,*** Left top panel: Representative images showing
793 archaerhodopsin T expression in MS and dorsal hippocampus reported by GFP. *Right top*
794 *panel:* Representative raw hippocampal LFP trace and spectrogram plot showing the effect
795 of MS yellow light stimulation on theta power. *Bottom panel:* Bars show mean hippocampal
796 theta (θ; 5-10 Hz), $_{S}$gamma (γ_S; 35-55 Hz) and $_{F}$gamma (γ_F; 65-100 Hz) power before, during
797 and after light delivery to the MS (n = 6 per group). Data expressed as median ± IQR or
798 mean ± SEM. *p<0.05, **p<0.01.
799
800 **Figure 4.** *Theta-burst stimulation of the fimbria-fornix induces artificial hippocampal theta-*
801 *gamma phase-amplitude coupling and restores the amnesic effect of reconsolidation*
802 *blockers in MS-inactivated animals.* ***A,*** *Top panels:* Schematic representation of fimbria-
803 fornix (FFx) stimulation protocols: theta stimulation (θ Stim.), theta-burst stimulation (TBS)
804 and high-frequency stimulation (HFS). *Bottom panels:* Animals received injections of

805 muscimol (MUS; 0.2 µg/side) into the medial septum (MS) and 15 min later the FFx pathway
806 was stimulated using θ, TBS or HFS protocols. Power spectrum density plots and
807 spectrograms show the effect of FFx stimulation on dorsal CA1 LFPs before and during FFx
808 stimulation. Dashed lines in spectrograms indicate stimulation intervals. ***B,*** Mean theta-
809 $_S$gamma (γ_S) and theta-$_F$gamma (γ_F) modulation index (MI) and representative phase-
810 amplitude comodulograms before and during FFx stimulation (n = 5 per group). ***C,*** PEX rats
811 were trained in the SDIA task (TR; 0.8 mA/2 s) 24 h after the last pre-exposition session and
812 one day later received MUS into the MS. Fifteen min after MUS infusion, the animals were
813 submitted to a 40 s-long non-reinforced memory reactivation session (RA) during which they
814 received no stimulation (No Stim.), theta stimulation in the FFx (θ Stim.) or TBS in the FFx
815 (RA). A group of PEX rats with electrode arrays implanted in dorsal CA1 ($RA_{(LFP)}$) was
816 treated and stimulated as animals in the RA group, except that LFPs were recorded
817 throughout the reactivation session. Additional control groups received TBS either in the FFx
818 during 40 s beginning immediately after memory reactivation (After RA), in the FFx during 40
819 s 24 h after training in the absence of RA (No RA), or in the corpus callosum during RA (C.
820 callosum). Five minutes after these manipulations, rats received bilateral injections of vehicle
821 (VEH; 0.9% saline) or anisomycin (ANI; 160 µg/side) into dorsal CA1. Retention was
822 evaluated one day later (TEST; n = 6-10 per group). ***D,*** *Left top panel:* Filtered LFPs and
823 normalized $_S$gamma and $_F$gamma amplitude distribution over theta; *Left bottom panel:* mean
824 theta-$_S$gamma and theta-$_F$gamma modulation index (MI) and representative phase-amplitude
825 comodulograms before and during RA; and *Right panel:* Spearman's r correlation
826 coefficients between test latency (median = 65, IQR = 27-364) and normalized theta power
827 (θ_{Power}; mean = 0.147, SEM = 0.024), $_S$gamma power ($\gamma_{S\ Power}$; mean = 0.072, SEM = 0.016),
828 $_F$gamma power ($\gamma_{F\ Power}$; mean = 0.019, SEM = 0.004), theta-$_S$gamma MI ($\gamma_{S\ MI}$; mean =
829 $0.792x10^{-3}$, SEM = $0.194x10^{-3}$) or theta-$_F$gamma MI ($\gamma_{F\ MI}$; mean = $1.164x10^{-3}$, SEM =
830 $0.216x10^{-3}$) during the reactivation session for the $RA_{(LFP)}$ animals that received ANI shown
831 in Fig 4C. ***E,*** PEX rats were trained and treated as in *C,* except that they received no

832 stimulation (No Stim.) or FFx TBS during RA (TBS) and 5 min later were given C/EBPβ
833 antisense oligonucleotides (ASO; 2 nmol/μl) or scrambled ASO (sASO; 2 nmol/μl) into dorsal
834 CA1 (n = 9 per group). Data expressed as median ± IQR or mean ± SEM. *p<0.05, **p<0.01,
835 ***p<0.001.
836
837 **Figure 5.** *Induction of artificial hippocampal theta-gamma phase-amplitude coupling during*
838 *RA overcomes the boundary conditions of avoidance reconsolidation and destabilizes*
839 *reconsolidation-resistant memories.* ***A,*** *Left panel:* HAN animals were trained in the SDIA
840 task (TR; 0.8 mA/2 s) 24 hours after the last handling session and one day later submitted to
841 a 40 s-long non-reinforced memory reactivation session during which they received no
842 stimulation (No Stim.) or FFx TBS (RA). A group of HAN rats with electrode arrays implanted
843 in dorsal CA1 was treated and stimulated as animals in the RA group, except that LFPs were
844 recorded throughout the reactivation session ($RA_{(LFP)}$). Additional control groups received
845 TBS in the FFx during 40 s beginning immediately after memory reactivation (After RA) or
846 TBS in the FFx during 40 s 24 h after TR in the absence of RA (No RA). Immediately after
847 these manipulations, rats were given bilateral intra-CA1 injections of vehicle (VEH; 0.9%
848 saline) or anisomycin (ANI; 160 μg/side) and retention was evaluated one day later (TEST; n
849 = 8-9 per group); *Central top panel:* Filtered LFPs and normalized $_{S}$gamma and $_{F}$gamma
850 amplitude distribution over theta; *Central bottom panel:* mean theta-$_{S}$gamma and theta-
851 $_{F}$gamma modulation index (MI) and representative phase-amplitude comodulograms before
852 and during RA (theta-$_{S}$gamma MI: $t(8) = 3.748$, $P = 0.0056$; theta-$_{F}$gamma MI: $t(8) = 5.548$, P
853 = 0.0005 for Before RA vs During RA in paired t test); and *Right Panel:* Spearman's r
854 correlation coefficients test latency (median = 101, IQR = 40-391) and normalized theta
855 power (θ_{Power}; mean = 0.342, SEM = 0.056), $_{S}$gamma power ($\gamma_{S\ Power}$; mean = 0.060, SEM =
856 0.011), $_{F}$gamma power ($\gamma_{F\ Power}$; mean = 0.023, SEM = 0.005), theta-$_{S}$gamma MI ($\gamma_{S\ MI}$; mean
857 = 0.670×10^{-3}, SEM = 0.154×10^{-3}) or theta-$_{F}$gamma MI ($\gamma_{F\ MI}$; mean = 1.019×10^{-3}, SEM =
858 0.132×10^{-3}) during the reactivation session for the $RA_{(LFP)}$ animals that received ANI shown

in the *Left panel.* ***B,*** HAN rats were trained and treated as in *A*, except that they received no stimulation (No Stim.) or FFx TBS during RA (TBS) and 5 min later were given C/EBPβ antisense oligonucleotides (ASO; 2 nmol/µl) or scrambled ASO (sASO; 2 nmol/µl) into dorsal CA1 (n = 7 per group). Data expressed as median ± IQR or mean ± SEM. *p<0.05, **p<0.01, ***p<0.001.

Table 1. Step-down latency during SDIA training. Repeated pre-exposure to the SDIA training box decreased step-down latency at training, indicating learning of SDIA-related non-aversive information during pre-expositions, as reported in Radiske et al. (2017). Latencies did not differ between groups for the same behavioral condition. Data presented as mean ± SEM and analyzed using unpaired t-test or one-way ANOVA.

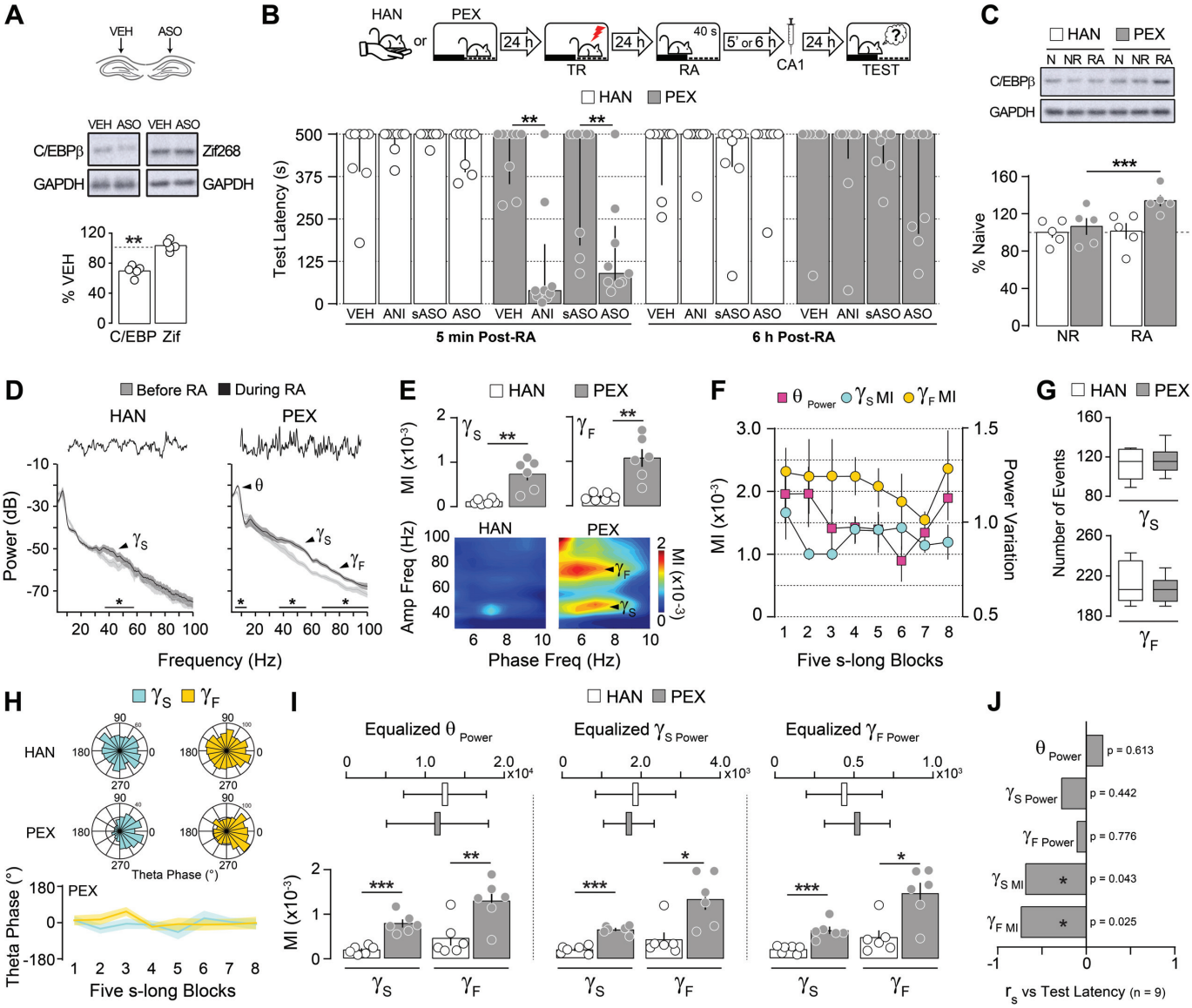

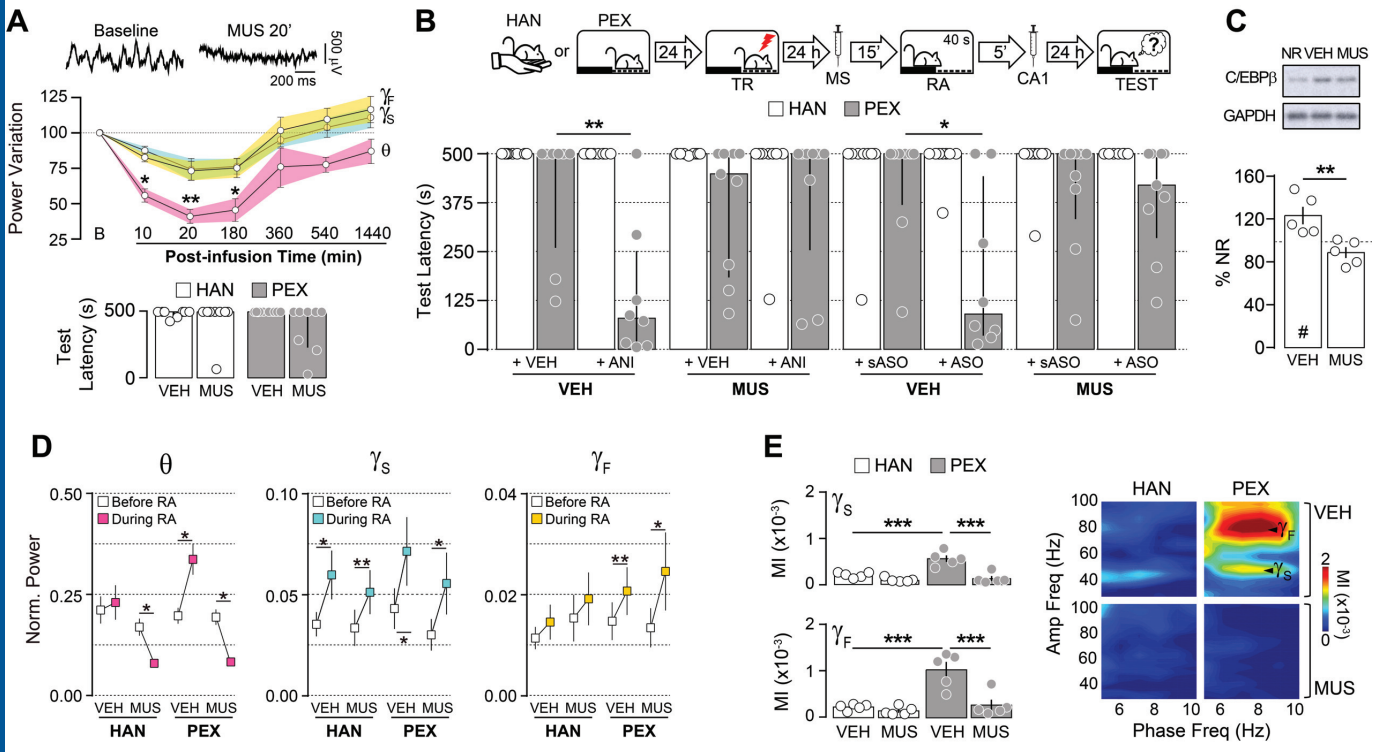

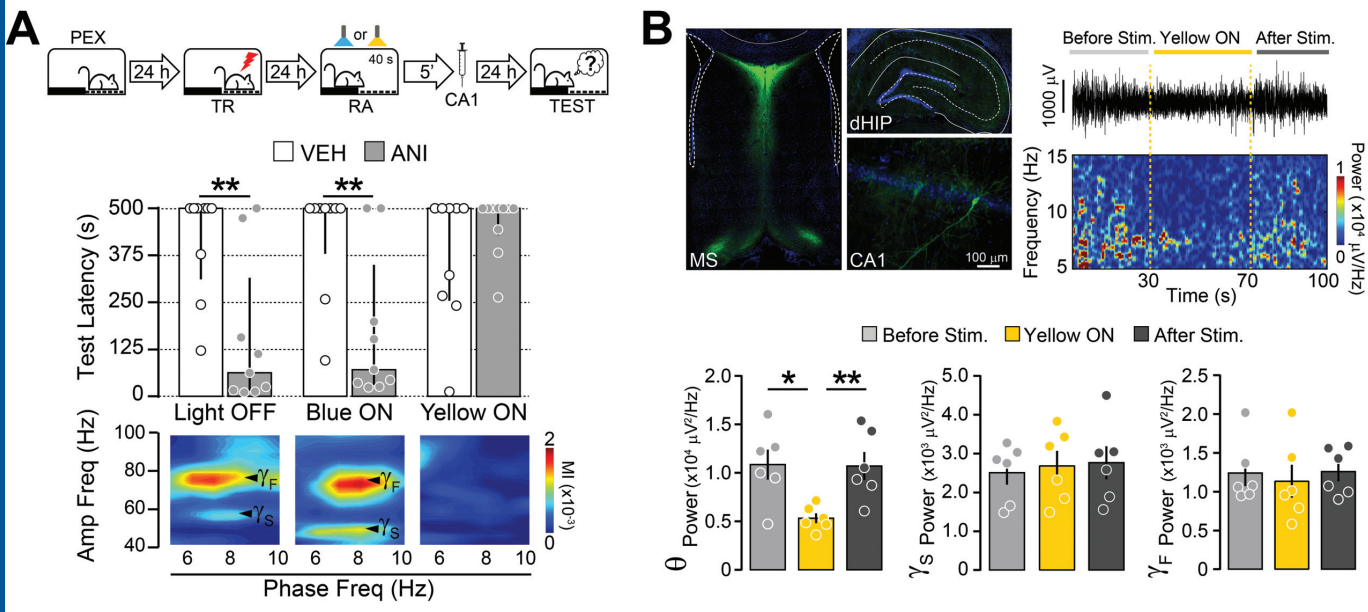

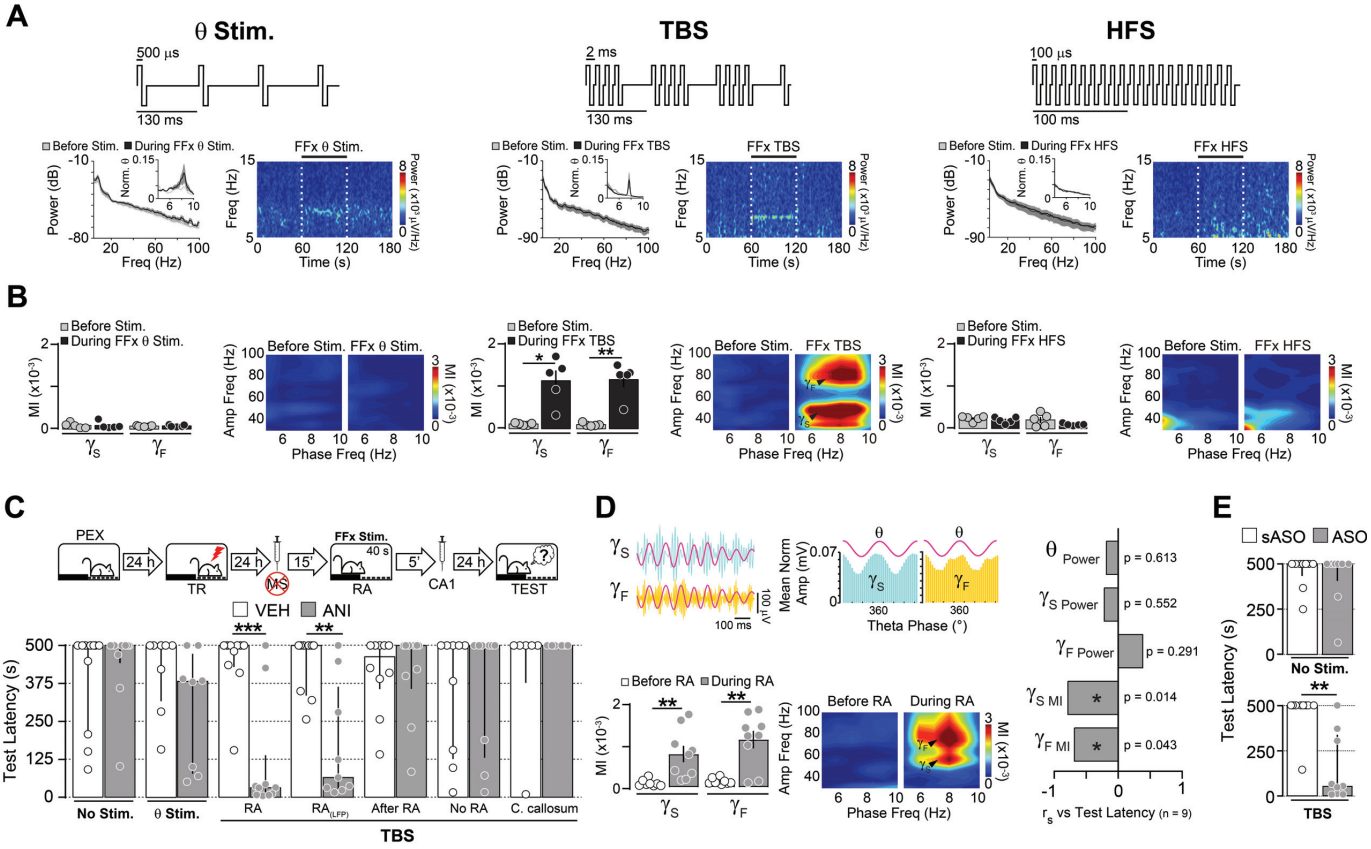

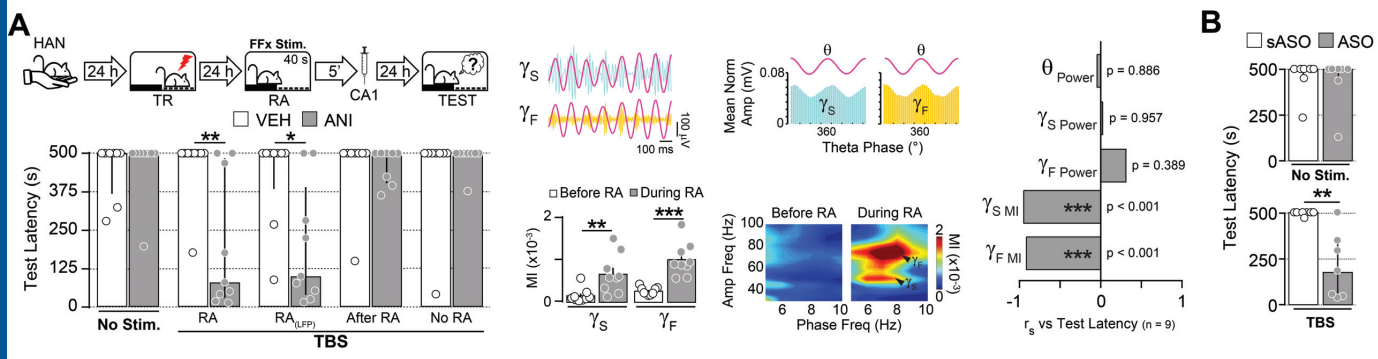

Table 1. Step-down latency during SDIA training						
Figure	**Behavioral condition**	**Treatment**	**Latency (s)** (per Group)	**n**	**Latency (s)** (per Condition)	**P** (HAN vs PEX)
1B	HAN	VEH 5'	11.75 ± 2.11	8	13.34 ± 0.93	< 0.0001
		ANI 5'	15.00 ± 2.77	8		
		sASO 5'	16.88 ± 2.68	8		
		ASO 5'	12.88 ± 2.66	8		
		VEH 6 h	12.25 ± 2.62	8		
		ANI 6 h	14.00 ± 3.47	8		
		sASO 6 h	11.88 ± 2.07	8		
		ASO 6 h	12.13 ± 3.03	8		
	PEX	VEH 5'	4.88 ± 0.85	9	5.68 ± 0.50	
		ANI 5'	5.00 ± 0.57	9		
		sASO 5'	7.44 ± 2.39	9		
		ASO 5'	5.88 ± 1.41	9		
		VEH 6 h	5.55 ± 1.58	9		
		ANI 6 h	4.66 ± 1.29	9		
		sASO 6 h	7.00 ± 1.70	9		
		ASO 6 h	5.00 ± 1.25	9		
1D-I	HAN	-	12.67 ± 1.58	6	-	0.0132
	PEX	-	5.33 ± 1.85	6	-	
1J	PEX	VEH	6.22 ± 1.02	9	-	-
		ANI	6.11 ± 1.30	9		
2A	HAN	VEH	13.25 ± 1.27	8	12.81 ± 0.91	< 0.0001
		MUS	12.38 ± 1.37	8		
	PEX	VEH	5.12 ± 0.85	8	5.37 ± 0.52	
		MUS	5.62 ± 0.65	8		
2B	HAN	VEH + VEH	11.00 ± 1.43	8	14.98 ± 0.89	< 0.0001
		VEH + ANI	15.63 ± 2.71	8		
		MUS + VEH	15.13 ± 2.72	8		
		MUS + ANI	17.13 ± 2.81	8		
		VEH + sASO	12.63 ± 2.41	8		
		VEH + ASO	16.25 ± 2.44	8		
		MUS + sASO	15.38 ± 2.51	8		
		MUS + ASO	16.75 ± 3.29	8		
	PEX	VEH + VEH	6.00 ± 1.64	8	6.08 ± 0.49	
		VEH + ANI	5.12 ± 0.63	8		
		MUS + VEH	5.11 ± 0.73	9		
		MUS + ANI	6.22 ± 1.09	9		
		VEH + sASO	7.87 ± 2.67	9		
		VEH + ASO	6.12 ± 1.58	8		
		MUS + sASO	6.11 ± 1.36	9		
		MUS + ASO	7.33 ± 1.40	9		
2D-E	HAN	VEH	13.40 ± 2.65	5	14.40 ± 1.78	< 0.0001
		MUS	15.40 ± 2.58	5		
	PEX	VEH	3.80 ± 0.66	5	4.80 ± 0.71	
		MUS	5.80 ± 1.58	5		
3	PEX	Light OFF / VEH	6.77 ± 1.913	9	-	-
		Light OFF / ANI	6.00 ± 0.897	9		
		Blue ON / VEH	5.77 ± 1.362	9		
		Blue ON / ANI	5.66 ± 0.866	9		

		Yellow ON / VEH	5.88 ± 1.814	9		
		Yellow ON / ANI	5.50 ± 1.327	10		
4C-D	PEX	No Stim. / VEH	6.80 ± 1.04	10	-	-
		No Stim. / ANI	6.90 ± 1.56	10		
		Theta Stim. / VEH	6.50 ± 1.15	8		
		Theta Stim. / ANI	7.25 ± 1.26	8		
		TBS RA / VEH	6.70 ± 1.484	10		
		TBS RA / ANI	4.90 ± 0.604	10		
		TBS $RA_{(LFP)}$ / VEH	6.11 ± 1.160	9		
		TBS $RA_{(LFP)}$ / ANI	6.00 ± 1.384	9		
		TBS After RA / VEH	6.60 ± 1.50	10		
		TBS After RA / ANI	6.30 ± 1.10	10		
		TBS No RA / VEH	6.66 ± 0.95	9		
		TBS No RA / ANI	5.88 ± 1.20	9		
		TBS C. callosum / VEH	6.16 ± 1.10	6		
		TBS C. callosum / ANI	5.66 ± 1.33	6		
4E	PEX	No Stim. / sASO	4.77 ± 0.70	9	-	-
		No Stim. / ASO	6.33 ± 0.95	9		
		TBS RA / sASO	5.55 ± 1.40	9		
		TBS RA / ASO	4.77 ± 0.87	9		
5A	HAN	No Stim. / VEH	10.88 ± 1.65	8	-	-
		No Stim. / ANI	12.38 ± 1.61	8		
		TBS RA / VEH	15.67 ± 2.02	9		
		TBS RA / ANI	13.89 ± 2.70	9		
		TBS $RA_{(LFP)}$ / VEH	12.11 ± 1.95	9		
		TBS $RA_{(LFP)}$ / ANI	15.67 ± 2.37	9		
		TBS After RA / VEH	9.87 ± 1.99	8		
		TBS After RA / ANI	14.50 ± 1.91	8		
		TBS No RA / VEH	11.50 ± 2.00	8		
		TBS No RA / ANI	12.25 ± 1.57	8		
5B	HAN	No Stim. / sASO	12.71 ± 1.61	7	-	-
		No Stim. / ASO	11.71 ± 2.56	7		
		TBS RA / sASO	15.00 ± 1.79	7		
		TBS RA / ASO	11.71 ± 2.48	7		